Soft Matter

PAPER

View Article Online
View Journal | View Issue

Cite this: *Soft Matter*, 2020, **16**, 9799

Investigation of the swollen state of Carbopol molecules in non-aqueous solvents through rheological characterization†

Simona Migliozzi, Giovanni Meridiano, Panagiota Angeli * and Luca Mazzei *

We explore how different types of solvent influence the rheological properties of non-aqueous Carbopol dispersions from the dilute to the jammed state. In novel non-aqueous formulations, polar solvents are used more and more frequently, because they can form Carbopol microgels without the need of any neutralizing agents. However, the swelling behaviour of Carbopol molecules in the absence of water, when ionic forces are weak, is still poorly understood. To this end, we study the swelling behaviour of Carbopol 974P NF in different polar solvents, *i.e.* glycerol, PEG_{400} and mixtures of the two solvents, by mapping the rheological behaviour of Carbopol suspensions from very dilute to highly concentrated conditions. The rheological study reveals that the onset of the jamming transition occurs at different critical polymer concentrations depending on the solvents used. Nevertheless, once the jammed state is reached, both elastic and yielding behaviours are scalable with the particle volume fraction. These results suggest that the type of solvent influences the final volume of the single Carbopol particles but does not alter the interactions between the particles. The final radius of the swollen particles is estimated from shear rheology measurements in dilute conditions, showing a decrease of the final swelling ratio of Carbopol molecules of almost 50% for PEG_{400} solutions, a result that confirms the shift to higher values of the critical jamming concentration obtained from linear viscoelasticity for the same solutions.

Received 30th June 2020,
Accepted 24th September 2020

DOI: 10.1039/d0sm01196g

rsc.li/soft-matter-journal

1 Introduction

In the past decades, the scientific and technological relevance of microgel suspensions has motivated extensive experimental and theoretical research.[1,2] These systems are formed by cross-linked polymeric molecules, usually of colloidal dimension, which swell when dispersed in an appropriate solvent, creating a suspension of soft elastic particles. As a result of this polymer-colloid duality, microgel suspensions present a unique phenomenology that unifies the rheological behaviour of hard colloidal spheres and polymeric macrogels,[3,4] a characteristic that makes them extremely valuable in a wide range of industrial and scientific applications. In the study of these suspensions, there has been great interest in particle–particle interactions[5–8] and in the properties of the individual polymer particles[9–12] (*i.e.*, chemistry and crosslinking structure), because both influence the macroscopic behaviour of microgel suspensions and can potentially provide a path towards the design of novel formulations.

Microgels that have received special attention owing to their wide industrial use are carbomers, also known with the commercial name of Carbopol. These molecules are high molecular weight polymers of polyacrylic acid crosslinked with polyalkenyl ethers or divinyl glycol.[13] Because of their nontoxicity, stability, high thickening properties and transparency, these polymers have been widely employed in cosmetics and pharmaceutical applications[14,15] as well as model yield stress fluids in academia.[16–19]

In the vast majority of applications, Carbopol preparations are water-based. In water, the molecule swelling is induced by the dissociation of acrylic acid, which constitutes the monomeric unit of Carbopol. Typically, a base is added during the preparation to neutralise the acidic groups, a process that causes the ionization of the carboxylate groups. Similar to most polyelectrolytes, the final swollen configuration depends on the

Department of Chemical Engineering, University College London, Torrington Place, London WC1E 7JE, UK. E-mail: l.mazzei@ucl.ac.uk, p.angeli@ucl.ac.uk

† Electronic supplementary information (ESI) available: Details of sample preconditioning; additional confocal images and summary of all concentrations tested; derivative of the loss moduli close to the jamming transition and summary of the evolution of G' and G'' with Carbopol concentration; trend of the loss tangents $\tan\delta$ with Carbopol concentration; graphical representation of the determination of the yield strain γ_y obtained from LAOS; discrepancy between σ_y and σ_B as a function of Carbopol apparent volume fraction; Carreau-Yasuda fitting parameters; reversibility of the yielding behaviour near the jamming transition; determination of Mooney's equation parameters. See DOI: 10.1039/d0sm01196g

internal density of uncompensated ions on the polymer backbone: the larger the density of these ions, the higher the difference in osmotic pressure between the internal crosslinked network and the external environment. This imbalance promotes the diffusion of solvent molecules inside the coiled Carbopol molecule, a process that makes the particles swell.[20] The final system results in a clear suspension of soft elastic particles, whose final dimensions are controlled by the pH of the solution.[21–23]

The rheological properties of water-based Carbopol microgels in the concentrated regime have been investigated extensively for many types of Carbopol molecules,[17,20,24,25] showing a typical soft glass behaviour, which can be described macroscopically by the Herschel–Bulkley constitutive equation.[17,23,26] Nonetheless, some discrepancies, mainly in the form of thixotropic behaviour,[27–29] were observed for systems that experienced different preparations, showing that the yielding behaviour of these systems is strongly influenced by changes in the internal microstructure,[19,21,30] changes that can be induced by different preparation protocols or by the presence of additives.[13,31,32] This aspect becomes particularly relevant in the development of novel non-aqueous formulations, where the combined effect of different solvents is difficult to predict.

Specifically, the use of organic solvents, instead of water, is important for various pharmaceutical applications that require addition of water-insoluble drugs or of active components which require *in situ* activation *via* water.[33] The swelling behaviour of Carbopol molecules in the absence of water, when ionic forces are weak, is still poorly understood. It is known that some polar solvents, such as glycerol and poly(ethylene glycols) of low molecular weight, can initiate the swelling without the use of neutralising agents.[34,35] This suggests that (i) polar solvents dissociate part of the carboxyl groups constituting the Carbopol backbone, thus unbalancing the osmotic pressure between the inside and the outside of the macromolecule and initiating the swelling process; (ii) compared to water, the organic nature of the solvents ensures a greater affinity with the Carbopol network, which promotes the internal diffusion of the solvent molecules even at low degree of dissociation. In these cases, the dimensions of the solvent molecules and their affinity with the carbomer structure can affect the final swollen conformation and alter the strength of colloidal interactions between microgel particles. The effect of co-solvents on the final properties of Carbopol dispersions has been investigated by some authors,[15,34,36] showing differences in the viscoelastic response of the material, yet no coherent analysis has been made in terms of how different solvents affect the swelling of Carbopol molecules and their interactions and how the rheological properties can be scaled accordingly.

In this work we seek to investigate the effect of polar solvents on the swelling and mutual interaction of Carbopol molecules and understand how these phenomena might impact the rheological design of novel non-aqueous formulations employing co-solvents. To this end, we study the rheology of dispersions of Carbopol 974P NF (C974P NF) in three different media, (i) poly(ethylene glycol) M_W = 400, (ii) glycerol and (iii) a 50/50 wt% mixture of the two solvents, by mapping the behaviour from dilute to highly concentrated conditions. Thanks to the high crosslinking density of C974P NF, the molecules are expected to maintain a well defined particle identity even when they are swollen, an attribute that allows rationalizing the rheological properties of the dispersions in the framework of soft particle suspensions. For all solvents, we conducted small-amplitude oscillatory tests to characterise the onset of the jamming transition in the three different media. These were followed by large-amplitude sweeps and steady shear tests to investigate the changes in the particle–particle interactions that different solvents might induce on the yielding of the suspensions. Studying the yielding behaviour of microgel systems has proven to be extremely valuable for identifying the driving mechanism of their liquid-to-solid transition, distinguishing between a purely cage-driven process, typical of repulsive glasses,[37,38] and a bond-driven process, triggered by particle–particle attractions.[39–41] In the absence of free ionic charges and polymer additives, the solvent type can affect the interparticle interactions in different ways, *e.g.*, altering the repulsion between electric double layers, through a change of the dielectric constant of the solvent or affecting the steric stabilisation of the particles through the strength of solvation.[42] In the case of commercial molecules such as Carbopols, predicting or characterizing rigorously how different solvents affect the interparticle interactions is arduous. Hence, we limited our study to finding evidence of changes in the interparticle interactions which could significantly alter the liquid-to-solid transition of C974P NF molecules dispersed in different solvents. Finally, the dimensions of swollen Carbopol particles in each medium were estimated from viscosity measurements conducted in dilute conditions and compared with direct observations of swollen unconfined Carbopol molecules through fluorescence confocal imaging.

The paper is structured as follows: in Section 2 materials and descriptions of samples preparation are first presented, followed by details of the experimental methods. In Section 3 all the rheological results are shown and discussed. Conclusions are given in Section 4.

2 Experimental methods

2.1 Materials and samples preparation

Carbopol 974P NF (C974P NF, Lubrizol Limited), the compound used in this study, is generally classified as a polymer of acrylic acid highly crosslinked with allyl pentaerythritol.[13] Carbopol dispersions in the range of polymer mass fractions between 0.15% and 8% were prepared in each of the three solvents mentioned: (i) poly(ethylene glycol) (PEG M_W = 400 Da, Sigma-Aldrich, UK), (ii) glycerol (purity > 99%, Sigma-Aldrich, UK) and (iii) a 50/50 wt% mixture of the two solvents.

The densities and viscosities of the solvents at ambient temperature (T = 25 °C) are reported in Table 1 together with the apparent density ρ_p and the hydrodynamic diameter R_{IN} of the unswollen Carbopol particles. ρ_p was detrmined by picnometry in hexane (Reagent grade ≥ 99%, Honeywell) to preserve the internal dry state of the unswollen particles,[20] whilst R_{IN}

Table 1 Raw materials properties at ambient temperature (T = 25 °C)

	ρ (g cm^{-3})	η_s (Pa s)		ρ_p (g cm^{-3})	R_{IN} (nm)
G	1.2559	0.815			
P	1.1218	0.0935	C974P NF	1.24 ± 0.004[a]	137 ± 37[b]
PG	1.1889	0.353			

[a] The error is the standard deviation calculated on three different measurements. [b] The error is the standard deviation of the distribution evaluated through DLS.

was determined through dynamic light scattering (DLS) measurements, performed using a DelsaMax-Pro DLS analyzer (Beckman Coulter, Brea, CA, USA) at 25 °C. For these tests, Carbopol was dispersed in isopropanol (Certified AR for analysis, Fischer Chemical) to prevent particle aggregation and consequent settling for the duration of the test and at the same time prevent any swelling. In fact, alcohols can swell Carbopol molecules only in the presence of a neutralising agent.[34] Tests repeated on the same sample after one week confirmed the particle dimensions obtained in the first instance, corroborating the absence of any swelling.

Carbopol molecules can swell in the absence of a neutralizing agent in all three solvents chosen; therefore, to ensure samples were reproducible, it was crucial to disperse the polymer homogeneously into the liquid phase before significant swelling occurred. Since Carbopol swells more slowly in PEG_{400},[35] the polymer powder was first dispersed in PEG_{400} at a controlled temperature of 20 °C, using a high-shear mixer (Silverson, L5 Series) working at 7000 rpm for approximately five minutes; then, the concentrated dispersions were diluted with PEG_{400} or PEG_{400}/glycerol mixtures to reach the final concentrations required. After dilution, the solutions were gently mixed with a magnetic stirrer in small batches of 20 g until they fully homogenized (~10 s). The vials were then left overnight in an ultrasonic bath (SciQuip Ultrasonic bath, heated, 150 W) at 50 °C. Given the quick swelling response of Carbopol in glycerol, a different approach was required to prepare the samples in pure glycerol. First the glycerol was heated up with a stirred hot plate to reduce its viscosity and form a central vortex; at this point, the required amount of Carbopol was poured gradually to avoid lumps. Once all the Carbopol had been added, the magnetic stirrer was switched off and the solution was stirred with a mechanical stirrer at 800 rpm for 15 minutes and then left overnight at 150 rpm. At the end of the process the samples were perfectly clear and uniform. For the most diluted samples, a stock solution at 0.7 wt% of Carbopol in glycerol was prepared, as explained above, and then further diluted with glycerol to obtain the final samples with the correct Carbopol content. All samples were usually left at rest for a minimum of three days before conducting any rheological tests. For brevity from here on we refer to the final Carbopol dispersions in the three different solvents as P (PEG), G (glycerol) and PG (50/50 wt% PEG/glycerol) dispersions.

2.2 Rheological measurements

All rheological measurements were performed with an Anton Paar MCR302 stress-controlled rotational rheometer. The instrument was equipped with a Peltier plate to precisely control the operating temperature and a parallel plate geometry (OD: 40 mm) with sand blasted surfaces (surface roughness of 2 μm) to avoid slip effects. All tests were carried out with a gap of 900 μm at a constant temperature of 25 °C. To avoid solvent evaporation, sample menisci were sealed with silicon oil, which enabled reliable measurements on the same sample for more than 10 hours. We performed three different rheological tests: (i) small-amplitude oscillatory shear (SAOS) tests, (ii) large-amplitude oscillatory shear (LAOS) tests and (iii) steady shear tests. Before all tests, samples were pre-sheared at a constant shear rate of 100 1/s for 60 s and left to rest for 900 s, which we verified to be sufficient to remove any mechanical history and obtain reproducible data for all tests (see S1, ESI†).

SAOS experiments were carried out to obtain insights into the changes of the sample microstructure induced by different Carbopol concentrations and to find the characteristic concentration at which the liquid-to-solid transition takes place for the different solvents used. To this end, the viscoelastic response of the samples to a sinusoidal deformation with fixed amplitude in the linear regime (*i.e.*, γ = 0.6%) was recorded in the range of angular frequencies ω = 0.01–100 rad s^{-1} and the corresponding values of the storage (G') and loss (G'') moduli were measured. All samples showing a readable elastic response were then tested through oscillatory amplitude sweeps experiments to investigate their yielding behaviour. LAOS tests were performed with fresh samples at a constant angular frequency of 1 rad s^{-1} in the range of amplitudes γ = 0.001–1000%. To complete the analysis of the rheological properties in the limit of non-linear deformations, we performed steady shear experiments, applying constant shear rates $\dot{\gamma}$ from 0.001 to 1000 1/s and recording the shear stress σ once steady state was reached. Data gathered from the most diluted samples were used to estimate the dimensions of the swollen particles in the three media. Note that, since we used a parallel-plate geometry, all the steady shear rheological data presented in the following sections represent the true values of stress and viscosity obtained by applying the Weissenberg–Rabinowitsch correction to the raw experimental data.

2.3 Confocal fluorescence microscopy

Confocal fluorescence microscopy was implemented to obtain direct images of swollen Carbopol particles in unconfined conditions and compare the results with the rheological findings. To this end, diluted dispersions at 0.1 wt% of labelled Carbopol were prepared following the same procedure described in Section 2.1. Carbopol particles were chemically labelled with rhodamine-123 (R123 mitochondrial specific fluorescent dye, Sigma Aldrich, UK). The labelling reaction is based on the method described by Laguecir *et al.*[43] for uncrosslinked polyacrylic acid molecules. The method involves attaching two intermediaries, *n*-hydroxysulfisuccinimide sodium salt (Sigma Aldrich, UK) and 1-[3-(dimethylamino)-propyl]-3-ethylcarbodiimide (Sigma Aldrich, UK), to the C974P NF monomeric units. The intermediaries are then substituted by R123. The solution is then purified *via* dialysis and freeze dried.[44] The final labelled powder was provided by the group of Prof. Paul Bartlett (School of Chemistry, University of

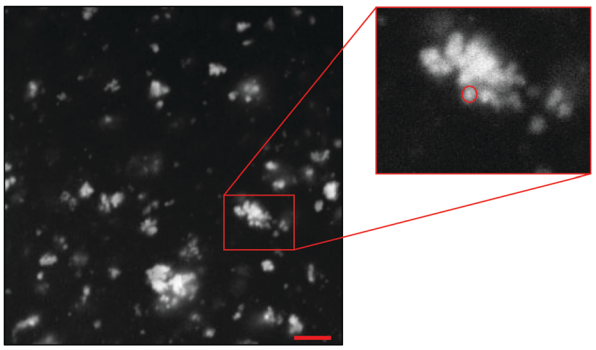

Fig. 1 Sample image obtained through confocal microscopy of 0.1 wt% labelled Carbopol swollen in glycerol. The scale bar indicates a dimension of 10 μm. The inset shows how single particles are identified manually. Particle radius is calculated as the radius of the equivalent circle covering the same pixel area.

Bristol, UK). The use of labelled Carbopol particles as opposed to the addition of a fluorescent dye in solution[13,22,45] allows distinguishing single particles and therefore measuring the average particle diameter of the swollen molecules. The diluted solutions were placed on a glass bottom dish (X20, Fischer Scientific, UK) and examined with a LSM 710 (Zeiss) confocal microscope equipped with an oil immersion objective (Plan-Apochromat 63x/1.4 Oil DIC M27, Zeiss). Samples were illuminated with an Argon laser (λ = 512 nm) with collected fluorescence bandwidth set to [519–682 nm]. A sample image obtained from Confocal microscopy is shown in Fig. 1. For all samples at 0.1 wt% of Carbopol, we observed a sparse particle phase where individual particles can be distinguished. Particles appear aggregated in small clusters, well dispersed in solution, showing an acceptable efficiency of the dispersion step (further images are shown in S2, ESI†). Confocal images reported by other authors at similar Carbopol concentrations in water with adjusted pH[13,22,28] are generally denser and in some cases present large connected areas. Besides the different protocol we used to tag the Carbopol molecules, as explained above, the dissimilar results may be due to a difference in the effective volume fraction of Carbopol in our samples, which is significantly lower than those reported in the literature. This is related to the smaller swelling degree obtained when Carbopol is not completely neutralised, as it is in our case, as opposed to the cases reported above, where an optimal amount of neutralising agent was always added in solution to reach the maximum swollen dimension attainable by the specific Carbopol molecule.

The images were analysed with Fiji-ImageJ software. Particles were identified manually, the areas (*i.e.*, the number of pixels occupied by each particle) were collected, and the radii, calculated as the radius of the equivalent circle that occupies the same area (Fig. 1), were used to create particle size distributions for different solutions. Particle sizes are at the limit commonly associated with colloidal particles ($\approx$1 μm)[46] and close to what is typically indicated by the manufacturer[21] or by other authors for C974P NF.[13] The average particle radii, estimated on a sample of 100 particles per solvent type, is of 660 $\pm$ 39 nm and 654 $\pm$ 26 nm for G and PG solutions, respectively. Within their standard deviations, the values are equal. A lower particle radius is found for P solutions (around 563 $\pm$ 15 nm). This result is based on a lower number of particles (around 20), given the higher difficulty to individuate single particles in this sample. These results suggest a reduction of the swollen particle dimension when only PEG_{400} is used, even though final conclusions cannot be drawn simply from this difference, which is too close to the limits of resolution of the images.

The swollen particle sizes obtained from the confocal images can be taken as a first particle size reference and used to evaluate the apparent particle volume fractions of the samples investigated. A table summarising all mass fractions implemented in the rheological investigations and corresponding apparent volume fractions can be found in the ESI† (S2). Given the uncertainties related to the particle dimensions and the great sensitivity to volume fraction of the rheological response of these systems, especially in the denser regimes, all data will be presented as a function of mass fractions and values of the corresponding apparent volume fractions ϕ will be given only as a gross indication of the extent of particle confinement.

3 Results and discussion

3.1 Linear viscoelastic properties – SAOS

Oscillatory tests at small amplitudes show a clear transition in the structural behaviour of the solutions upon increasing the amount of Carbopol (Fig. 2). For polymer mass fractions lower than 0.2 wt%, all suspensions present a purely viscous behaviour, with the loss modulus linearly proportional to the solvent viscosity (*i.e.*, $G'' \propto \omega\eta_s$) and the storage modulus undetectable (*i.e.*, $G' = 0$) in the entire range of frequencies tested. This indicates that below 0.2 wt% particle interactions are negligible and the macroscopic elastic properties of the suspensions are related solely to the elasticity and the thermal energy of the single particles.[4] This contribution is extremely small and can hardly be measured, resulting in a purely viscous behaviour. As the polymer concentration increases to mass fractions of 0.4 wt%, while P solutions still present a purely viscous behaviour, for G and PG solutions, which approximately have a particle volume fraction of 0.4 (see Table S2.2, ESI†), the particles contribution becomes more appreciable and the macroscopic elastic properties of the suspension can be detected. In this regime, particle interactions and confinements appear still negligible and the suspensions display the typical behaviour observed for a Maxwell fluid in the viscous limit (also referred to as terminal viscous regime), with $G' \propto \omega^2$ and $G'' \propto \omega$. This indicates that the longest relaxation time of the solutions is far smaller than the reciprocal of the highest frequency tested (*i.e.*, $De_{max} \equiv \lambda_{max}\omega_{max} \ll 1$, where De is the Deborah number).

For a further increase of mass fraction to 0.7 wt% (Fig. 2a), P solutions present the same terminal viscous regime observed for G and PG solutions at 0.4 wt%, whilst the G and PG solutions deviate from it, with the storage and loss moduli having a similar slope of 1 in the window of frequencies sampled.

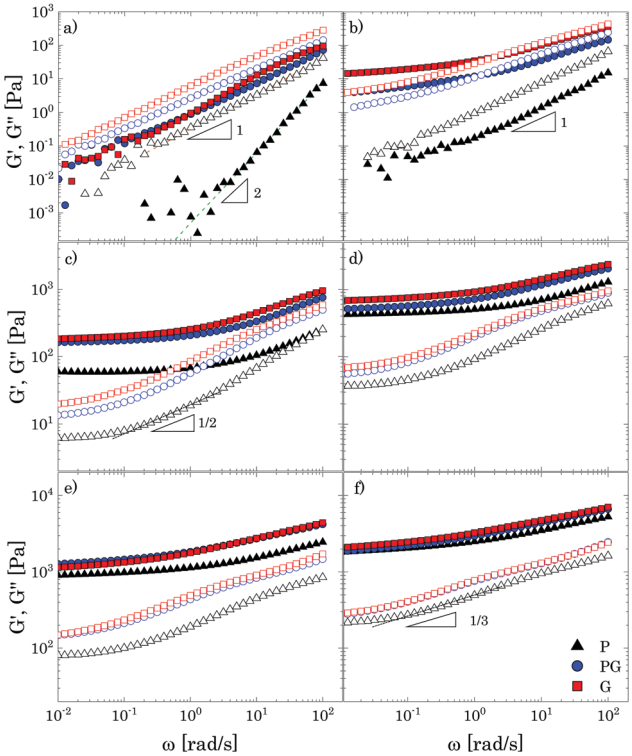

Fig. 2 Frequency dependence of the storage (closed symbols) and loss (hollow symbols) moduli in the three different solvents for increasing Carbopol concentrations: (a) 0.7 wt%; (b) 1 wt%; (c) 2 wt%; (d) 3 wt%; (e) 5 wt%; (f) 8 wt%. Dashed lines indicate the power law trends.

The viscous components are still higher than their elastic counterparts, but an anomalous power law of the storage modulus (1 instead of 2) is observed. The same behaviour is shown by P solutions at 1 wt% (Fig. 2b). The indicative apparent volume fractions associated with these conditions are between 0.6 and 0.7, indicating significant particle confinement; this entails a more complex response to linear deformations, because a local rearrangement of particles can propagate and cause a second rearrangement elsewhere in the material and so on. This leads to a distribution of relaxation times resulting in an anomalous macroscopic rheological response,[47] as seen in Fig. 2a.

At a Carbopol mass fraction of 1 wt%, G and PG solutions start to show a plateau of G' at low frequencies followed by a crossover where G'' slightly overtakes G'. This behaviour suggests that particle confinement is more significant than in P solutions, the G and PG solutions being closer to a disordered arrested state where particles are caged by their neighbours. As the G and PG solutions approach this state, their macroscopic elastic response becomes gradually controlled by the elasticity of the whole network of particles; consequently, the storage modulus gradually increases and the frequency interval in which it is constant widens. On the other hand, the viscous response is controlled by the viscous dissipation in the solvent, which arises from the superposition of the dissipation induced in the liquid by the particle motion and the dissipation induced in the liquid by the deformation applied to the sample externally. While the second contribution increases with the frequency monotonically, independently of the particle concentration, the first is significant only in a (low) range of frequencies related to the characteristic distribution of relaxation times $H_c(\lambda)$, which, in turn, is associated with the particles mobility. In particular, the dissipation induced by the particle motion is important when $\lambda_{min}\omega \ll 1$, where λ_{min} is the lowest value for which $H_c(\lambda)$ is significant. As particles are increasingly confined, their movements are more and more restricted and the contribution to the total viscous dissipation induced by particle motion becomes more significant. This entails that, in comparison with the purely viscous case, the total viscous dissipation in the solutions increases at lower frequencies, as observed by comparing the trend of G'' for G and PG solutions in Fig. 2a and b.

In a generic repulsive system of Brownian particles, by further increasing particle confinement, the system eventually reaches the onset of the glass transition, where particles are trapped in metastable cages formed by their neighbours. In these conditions, each particle can move in the cage with a characteristic time related to its Brownian motion, but it will only be able to escape its position for times exceeding those experimentally observable.[1] Hence, the viscous response in the glassy regime is dominated by the "outside the cage" motion (α-relaxation) at very low frequencies, usually unattainable in the range of experimental frequencies achievable, by the "in-cage" motion (β-relaxation) at intermediate frequencies ($\lambda_{min}\omega \ll 1$), and by the viscous dissipation induced in the solvent by the external deformation at higher frequencies. This physical picture translates in a specific viscous response, which is typically characterised by the appearance of a minimum for G'' in the range of frequencies experimentally accessible, associated with the characteristic relaxation time of the in-cage motion, followed by a power law increase with ω, where G'' gradually reaches G'. As the particle concentration is further increased, the in-cage motion is limited by the increased confinement of the particles, which are forced to contact, and the minimum shifts to lower frequencies. Hence, in the range of experimental frequencies, the profile of G'' flattens in the low-frequency region of the range (as G'' approaches the minimum) and the region dominated by the viscous dissipation caused by the externally-applied deformations extends. This marks the onset of the jamming transition, which, from the data depicted in Fig. 2c, appears to happen between Carbopol mass fractions of 1 and 2 wt% for all solutions. At 2 wt%, the plateau of G' extends to higher frequencies, whilst G'' tends to a shallow minimum at low frequencies (the first derivative of G'' is reported in S3.1, ESI†). Moving away from the minimum as the frequency is increased, G'' rises monotonically following a power law with a slope of 0.5. This trend, typical of randomly packed emulsions[48] and observed also for microgels close to the jamming transition,[10,49,50] is associated with the presence of regions where slip happens between loosely packed particles, which increases the viscous dissipation in the solvent at higher frequencies. This slip also implies the presence of a distribution of relaxation times, which, for randomly distributed dispersions,[48] yields a power

law dependence of the loss modulus of $\omega^{1/2}$. A clear distinction between the glass transition and the jamming transition is not observed from the trends of G' and G'' *versus* frequency in the range of concentrations investigated. This is likely to occur, because a clear distinction between the two phenomena can be attained only if the characteristic time of the test (which for SAOS experiments corresponds to the reciprocal of the frequency of oscillation, *i.e.* $1/\omega$) is longer than the characteristic time of Brownian motion,[51] which can be evaluated as:

$$\tau_T = \frac{(3\pi\eta_s a^3)}{k_B T} \quad (1)$$

where a is the average particle diameter (*i.e.* $2R_{SW}$, where R_{SW} is the radius of the swollen Carbopol particle), k_B is the Boltzmann constant and T is the operating temperature. Using the rough particle diameter obtained from confocal microscopy, we obtain values of τ_T equal to $4.3 \times 10^{+3}$ s, $1.8 \times 10^{+3}$ s, $3 \times 10^{+2}$ s for G, PG and P solutions, respectively. Hence, to sample the thermal contribution of the particles, experimental oscillations lower than 10^{-3} Hz should be sampled, which are below those reached in the experiments.

Moving towards more concentrated samples, for all solvents the viscoelastic properties show the typical features of a densely packed system of soft particles. The storage modulus is nearly constant over the range of frequencies sampled, with a mild increase at high frequencies, and the gap between the P and G/PG solutions gradually decreases, their respective curves almost overlapping at the highest concentration considered (*i.e.* 8 wt%; Fig. 2f). This behaviour reflects the ability of these microgel particles to deform when highly compressed. As the particle density increases, the space occupied by the solvent is gradually filled with polymer. In these conditions, the elastic response is controlled by the particle elastic modulus G_p, which primarily depends on the chemistry of the crosslinked system,[52] thus yielding (in a log scale plot) close values of G' for the three solutions. As the interstitial spaces between particles decrease, G' and G'' increase, the ratio G'/G'' increases, and the power law dependence of G'' at higher frequencies reduces to $\omega^{1/3}$. The decrease of the power law exponent agrees with studies on microgels systems above the jamming transition[10,50,53] and could reflect the ability of soft polymer particles to deform and partially interpenetrate when compressed, a behaviour that promotes frictional effects between sliding particles.[50,53] Although direct observations of the compressed state of the system are unavailable, for all solutions a non-monotonic variation of the loss tangent is observed with an increase of Carbopol concentration at a fixed frequency, a finding that agrees with what is reported in the work of Conley *et al.*[50](see S4, ESI†): the loss tangent motonotically decreases with an increase of microgel concentration until reaching a minimum at the onset of the compressed state, after which it increases moderately approaching a plateau. The authors observed that the anomalous large losses scaled with the degree of interpenetration of the microgels, thus possibly associating the altered scaling behaviour of G'' with the presence of frictional forces between the compressed dangling ends of the microgels.

Based on the results discussed so far, the use of PEG_{400}, in contrast to the other two solvents, clearly induces a shift of the characteristic polymer mass fraction at which the liquid-to-solid transition occurs (close to 2 wt% for the P solutions and between 1% and 2% for the G and PG solutions), albeit no significant differences in the viscoelastic properties are observed once the dispersions become densely packed. This suggests that the solvent might influence mainly the final dimension of the swollen Carbopol particles.

A figure summarising the evolution of G' and G'' with Carbopol concentration can be found in the ESI† (S3.2).

To obtain a clearer picture of the liquid-to-solid transition and how it is influenced by solvent type, we considered the values of G' at a fixed frequency of 1 rad s^{-1} (G_0') and plotted them against the mass concentration of Carbopol per volume of suspension. The results are reported in Fig. 3, starting from Carbopol concentrations equivalent to a mass fraction of 0.4 wt% for G/PG and 0.7 wt% for P solutions (at 0.4 wt% the signal of G' for P solutions is significantly scattered at a frequency of 1 rad s^{-1}); at these low mass fractions, the values of G_0' are very low, in line with the viscous behaviour observed in Fig. 2. At intermediate concentrations (from 0.7 wt% to 1.5 wt% for G and PG solutions and 1 wt% to 2 wt% for P solutions), G_0' increases steeply for all solutions (hollow symbols in Fig. 3). Interestingly, values for PG and G solutions clearly overlap in the entire window, while the values for P solutions are shifted to higher Carbopol concentrations.

The rapid increase of the storage modulus is reported for a variety of colloidal and soft systems, from colloidal suspensions of hard spheres[12,54,55] and packed emulsions[56] to microgel systems,[4,8,10,12,50,57–59] and is typically associated with the

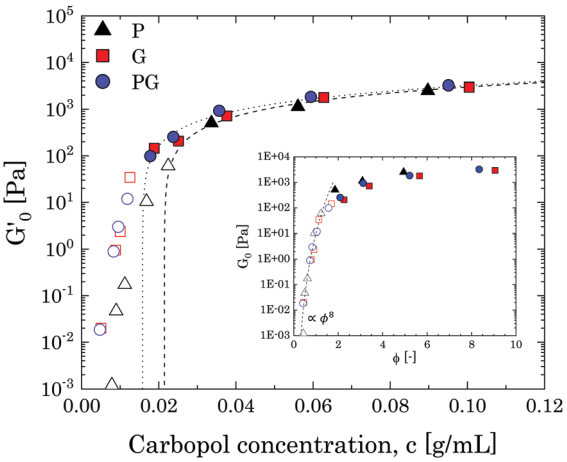

Fig. 3 Storage modulus (at ω = 1 rad s^{-1}) as a function of Carbopol concentration for P, G and PG solutions. The closed symbols are data above the jamming transition, whilst the hollow symbols are data below the jamming transition. The black dotted and dashed lines represent data fittings with the linear relation $G_0' = K_p(c - c_c)$. The inset shows the same data *versus* the apparent volume fraction ϕ in semilog scale. The line is a guide for the eye.

presence of a soft interaction potential between neighbouring particles, which appears to control the elastic behaviour of the system as this increasingly concentrates. Scheffold and co-workers[57] showed that soft microgels can be modelled considering the microgel particles as dense cores decorated with polymer brushlike coronas. Following this picture, the origin of the soft interactions can be attributed to brushlike interactions between close microgels, which strongly depend on the ratio between the particle diameter and the extension of the thickness of the coronas. This approach yields a distinct scaling behaviour for a specific microgel system, which can be approximated to a power law in a limited range of volume fractions. Although in this specific case a quantitative assessment is not feasible given the limited number of points in the range of interest, we notice that the data points in this intermediate regime can be collapsed for all solutions by simply using the apparent volume fraction evaluated from the confocal images. The results can be observed in the inset of Fig. 3 and show a common scaling which approximates a power law of 8, thus suggesting that the delay observed in the P solutions is ascribable to the smaller swollen dimension of the particles.

As the solutions concentrate further (from 1.5 wt% for G and PG solutions and from 2 wt% for P solutions), a smooth transition of G_0' is observed from the steep power law trend to an asymptotic linear increase with polymer concentration. This is commonly observed for microgel systems above the jamming transition and its physical interpretation from dynamic data is not unique.[60] The most common scenario considers the ability of soft particles to deform and adapt their shape as they are forced by the steric constraint of the other particles. In these conditions, particles form a dense, packed system, where the elastic behaviour is controlled by the physical properties of the microgel core.[4,10,50] In this regime, the plateau of the storage modulus is predicted to increase linearly with the particle volume fraction,[61] $G_0' = G_p(\phi - \phi_c)$, G_p being the particle elastic modulus, ϕ the particle volume fraction and ϕ_c the characteristic volume fraction corresponding to close packing. Assuming as a rough approximation a linear relation between the particle volume fraction ϕ and the mass concentration c (*i.e.* $\phi \approx k_M c$, where k_M is a proportionality constant) the equation above translates into $G_0' = K_p(c - c_c)$, where c_c is the close packing concentration, which marks the onset of a densely packed regime (*i.e.* regime in which particle deformations start to become significant and the onset of the linear behaviour is observed[50]) and K_p is a proportionality constant, independent of the solvent considered, related to the particle elastic modulus G_p by the relation $K_p = k_M G_p$. The estimated values of K_p and c_c can be obtained by linear regression of the data at the highest concentrations (closed symbols in Fig. 3), yielding a value of 38 $m^2\ s^{-2}$ for K_p and values of the characteristic concentration c_c of 0.0158 g mL^{-1} for G and PG solutions and of 0.0214 g mL^{-1} for P solutions, corresponding to Carbopol mass fractions of 1.25%, 1.3% and 1.9% for G, PG and P solutions, respectively, in line with what is shown in Fig. 2. Thus, the use of different solvents does not alter the interparticle interactions in the limit of small deformations, but it clearly influences the swelling behaviour of the Carbopol molecules, an outcome reflected in a shift in the P solutions to a higher c_c.

Note that the critical concentration c_c does not indicate the typical onset of the jamming transition, which by definition is the point at which a suspension of particles reaches the random packing volume fraction ϕ_J, but indicates the point at which significant particle deformation and contacts occur. The corresponding mass fraction at which the jamming transition happens cannot be clearly defined from linear viscoelasticity for a system of soft particles, where the actual volume fraction is not precisely defined. From the data obtained and based on the apparent volume fractions reported in the ESI† (S2.2), we can simply say that we expect the jamming transition to occur at mass concentrations between 1 wt% and c_c. We also point out that, based on the data obtained so far and on the rough estimates of the apparent volume fractions, the transition to a solid arrested state seems to be mainly "cage" driven for all solutions.

3.2 Rheological response to non-linear deformations – LAOS

To further examine the influence of solvent quality on the soft interactions between Carbopol particles and on the nature of the transition observed in the linear viscoelastic regime, we tested the response to non-linear deformations of different samples through large amplitude oscillatory sweeps (LAOS) and steady shear rheology. The yielding response of microgel systems strongly depends on the nature of the interparticle interactions and on the particle volume fraction; thus, the results obtained from both tests for samples that are significantly beyond the densely packed regime (*i.e.* all concentrations clearly belonging to the linear region in Fig. 3, $c \geq 3$ wt%) and below this threshold, will be discussed together to highlight possible differences induced in the particle–particle interactions by the solvents used.

3.2.1 Densely packed state. For densely packed systems (all samples with $c \geq 3$ wt%), the response to shear deformations is controlled by the elastic restoring force of the packed medium and the frictional forces between particle facets.[62] When the stress is high enough to overcome the restoring forces, particles can escape their positions at rest and slide against each other thanks to the presence of thin liquid films between the facets that allow a fluid-like response of the material under shear flow. Experimentally, when an increasing shear strain is applied, this mechanism entails a distinctive response of the loss and storage moduli as the material yields, which is characterized by a crossover between the two moduli and a maximum of G''. The peak of the viscous component is typically attributed to an increase of the viscous dissipative energy associated with particle rearrangement.[29,38] In the flow regime, after the yielding point, G' and G'' monotonically decrease with the amplitude of the strain applied following a power law dependence, *i.e.*, $G' \sim \gamma^{-\mu}$ and $G'' \sim \gamma^{-\nu}$, with $\mu/\nu \approx 2$. Fig. 4 shows the results from LAOS experiments at 1 rad s^{-1} for all Carbopol dispersions with $c > 3$ wt%.

All samples exhibit the main features described above, independently of the solvent used, thus confirming the results

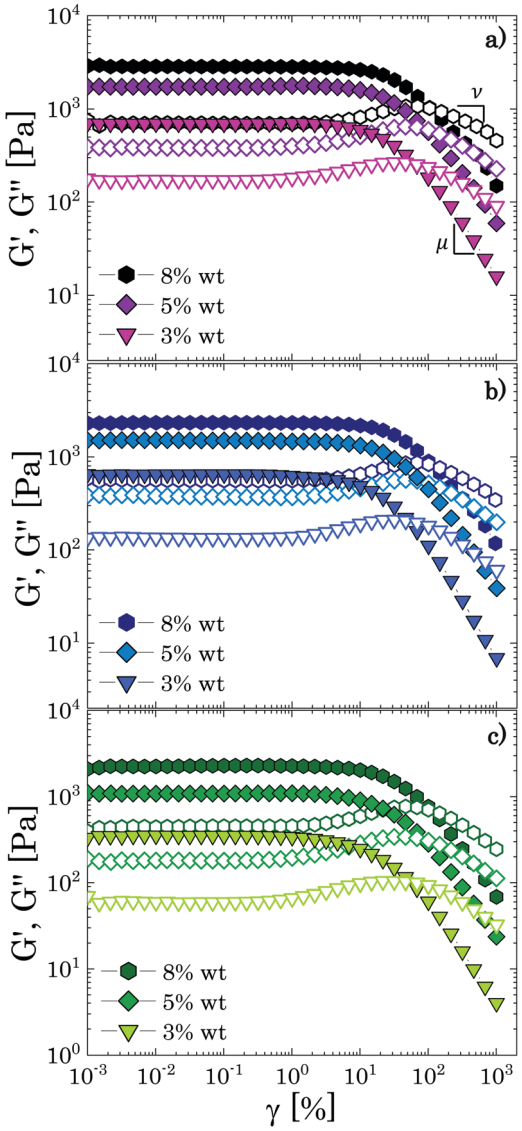

Fig. 4 Strain amplitude dependence of the storage (closed symbols) and loss (hollow symbols) moduli at ω = 1 rad s^{-1} for highly concentrated samples ($c \geq 3$ wt%) for the three different solvents obtained from LAOS experiments: (a) glycerol; (b) PEG/glycerol; (c) PEG.

obtained in the linear regime. Specifically, we found a mean value of the ratio/equal to 2.3 ± 0.2, a result that agrees with the value expected for soft glassy materials.[4,37,41] The values of the characteristic yield strain amplitude γ_y can be found from the analysis of stress (amplitude) *vs.* strain (amplitude) curves as the values at which the stress deviates from the linear elastic regime ($\sigma = G\gamma$) to a sublinear regime of the type $\sigma \sim \gamma^m$ with $0 < m < 1$ (see S5 ESI†). The data obtained for all samples are collected in Table 2 together with the estimated values of the yield stress $\sigma_y = G_0'\gamma_y$, and the characteristic power law exponents μ,ν and m.

The values of yield strain and consequently of yield stress obtained from the LAOS tests should not be considered as absolute thresholds between flow and no-flow conditions. As highlighted in the literature,[29,63,64] the yielding process of soft materials is not discontinuous, but a smooth transition from a completely structured to a completely unstructured state. As a consequence, various ways have been proposed to calculate the yield point from LAOS (at least five[29,63]), which give yield stress values that can differ significantly, thus highlighting the challenge of defining unambiguously the yield point from these tests.

As expected for a jammed glass, the exponent m remains constant with an average value of 0.45 ± 0.02 and the yield strain increases mildly with the polymer concentration, maintaining values between 10–30%, which is in the range found for various soft jammed systems in the densely packed regime.[38,41,60] Note that the high values observed at the highest mass fractions (5 wt% and 8 wt%) might highlight that the yielding behaviour in this regime is dominated by the elastic forces exerted at the particle facets, rather than by the elasticity of the particle cages.[38] By plotting the values found for γ_y as a function of the apparent volume fraction (Fig. 5a), we can also observe qualitatively a unique trend for all solutions where γ_y increases almost linearly with the volume fraction, an outcome consistent with the predictions for jammed Hertzian elastic particles.[65]

The typical yielding behaviour of jammed glasses is also recovered through steady shear measurements, as can be observed from Fig. 6, where stress *vs.* shear rate curves are presented for the same samples discussed above. All flow curves can be modelled with the Herschel–Bulkley (HB) constitutive equation:

$$\sigma = \sigma_B + k_n\dot{\gamma}^{n_B} \quad (2)$$

where σ_B, k_n and n_B are the fitting parameters of the model. Values of the parameters for all samples in the fully packed regime are collected in Table 2. An interesting result is given by the values found for the power law coefficient n_B, which are all close to 0.5 (the average value considering all samples is 0.485 ± 0.04), this being the value commonly found experimentally[4,66] and predicted theoretically for soft particle glasses above the jamming transition.[67] We note that the yield stress values found through the fitting of the steady shear measurements, σ_B, are always lower than the values found through LAOS experiments. The discrepancy reduces as the system moves away from the densely packed regime, until it reaches very close values at concentrations closer to c_c. This is depicted in Fig. 5b, where σ_B and σ_y are reported as a function of Carbopol concentration for PG solutions (the same behaviour is observed for the other two solvents, S6, ESI†). Although small differences between the two quantities have been observed in the literature in similar systems[60] and might be in part related to the ambiguity of the yield stress definition from the LAOS experiments, the trend observed in Fig. 5b suggests that the discrepancy might be related to interactions between squeezed dangling ends of the microgels, which, in extremely dense regimes, can interpenetrate, thus locally creating stronger interconnections between particles that enhance the threshold required to yield the sample when a finite deformation is applied (as in the case of LAOS). The morphology of Carbopol particles is in fact highly irregular,[19] allowing the particles to

Table 2 Experimental parameters evaluated from the LAOS tests and values of the HB parameters obtained from fitting of the experimental flow curves in the densely packed state. Values of γ_y are extrapolated from the analysis of stress *vs.* strain curves as depicted in Fig. S5.1 (ESI). G_0' values represent the plateau of G' in the linear viscoelastic region (Fig. 4) and the yield stress σ_y is calculated as $\sigma_y = G_0'\gamma_y$

w_c (%)		γ_y (%)	σ_y (Pa)	m (−)	μ (−)	ν (−)	G_0' (Pa)	σ_B (Pa)	k_n (Pa s^{n_B})	n_B (−)
8	G	38	903	0.48	1.16	0.44	2834	259	1102	0.46
	PG	23	699	0.42	0.93	0.46	2332	223	916	0.54
	P	31	624	0.42	1.08	0.55	2279	197	671	0.44
5	G	30	527	0.46	1.13	0.47	1732	131	544	0.47
	PG	22	346	0.42	1.04	0.49	1503	127	496	0.44
	P	18	202	0.43	1.13	0.51	1087	87	158	0.51
3	G	22	155	0.45	1.25	0.53	696	55	166	0.51
	PG	13	85	0.46	1.15	0.49	648	39	163	0.48
	P	12	44	0.46	1.22	0.52	351	29	61	0.51

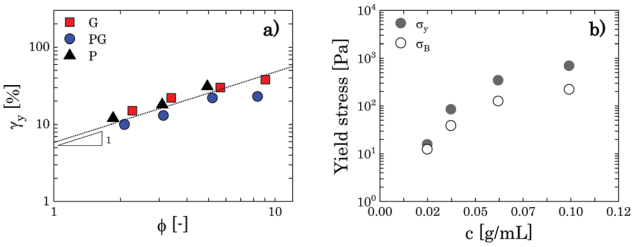

Fig. 5 (a) Yield strain as a function of the apparent volume fraction ϕ for G, PG and P solutions in the densely packed regime (the values corresponding to 2 wt% of Carbopol in G and PG solutions are also added). The dotted line is a guide for the eye and indicates a slope of 1 in the log–log plot. (b) Discrepancy between σ_y and σ_B as a function of Carbopol concentration for PG solutions in the densely packed regime.

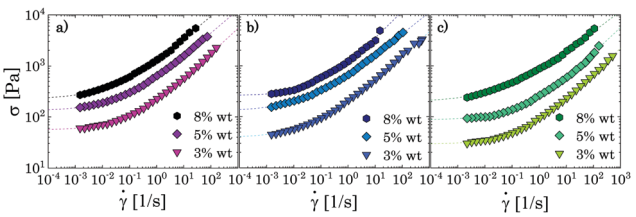

Fig. 6 Flow curves of the samples in the densely packed regime for the three different solvents: (a) glycerol; (b) PEG/glycerol; (c) PEG. The dashed lines represent the fitting of the experimental data with the Herschel–Bulkley model.

strongly deform, squeeze and interpenetrate when forced at high compression levels.

Hence, from all the results above, it can be concluded that the use of different solvents does not influence the qualitative behaviour of the flow properties of the suspensions when these are densely packed, thus confirming that, in this regime, particle interactions are mainly elastic and flow results from an interplay between the elastic interaction between particles in direct contact and structural rearrangements. In these conditions, any mild attractive force induced by a specific solvent is overwhelmed by the elastic interaction. Therefore, it is necessary to analyse the nonlinear response of less concentrated samples before drawing conclusions on the effect of the different solvents on the liquid-to-solid transition of Carbopol dispersions.

3.2.2 Below the densely packed state. When the Carbopol concentration is reduced to values closer to the jamming transition, the effective particle volume fraction in solution decreases, approaching the typical value for random packing (0.64–0.75 depending on the polydispersity of the powder). At these volume fractions, the interstitial spaces between the particles increase and the nature of the interparticle interactions begins to play a crucial role in the flow behaviour of the dispersions and the way particles escape their positions at rest to rearrange when large deformations are applied. Fig. 7 reports the responses of G' and G'' from LAOS tests as the concentration approaches the critical condition c_c and is further reduced below this threshold for the three different solvents. At the highest concentration plotted (2 wt%), the trends of both moduli for PG and G solutions present the same behaviour observed in the previous section for higher concentrations; this is expected since the concentration is still higher than the critical value c_c, indicating that particles are still significantly confined and possibly deformed. However, the peak of G'' appears less pronounced and wider compared to the more concentrated cases. The crossover between G'' and G' is slightly delayed towards higher strains, roughly in the middle of the flat region of the peak of G''. These observations hint at the formation of a second peak in the loss modulus, which is usually observed for colloidal systems close to the jamming transition presenting attractive interactions (attractive glasses).[39,41] The typical physical picture of the yielding behaviour of these systems is described as a cascade of events: at increasing oscillatory strain, first particle–particle interactions are disrupted; this implicates a peak of G'' at a value $\gamma = \gamma_{c1}$ (with $\gamma_{c1} \approx 10\%$), which is linked to the energy dissipated by bond breaking, and an initial decrease of G', due to local particle rearrangement. Then, for a further increase of the strain applied, particle cages break ($\gamma = \gamma_{c1} \approx 100\%$) and particles are free to escape their positions[41,68] giving rise to a second peak of G'' and to the terminal power law decrease of G'. As particle volume fraction is decreased below the jamming point, at fixed interparticle interactions, the position of the second peak moves to higher

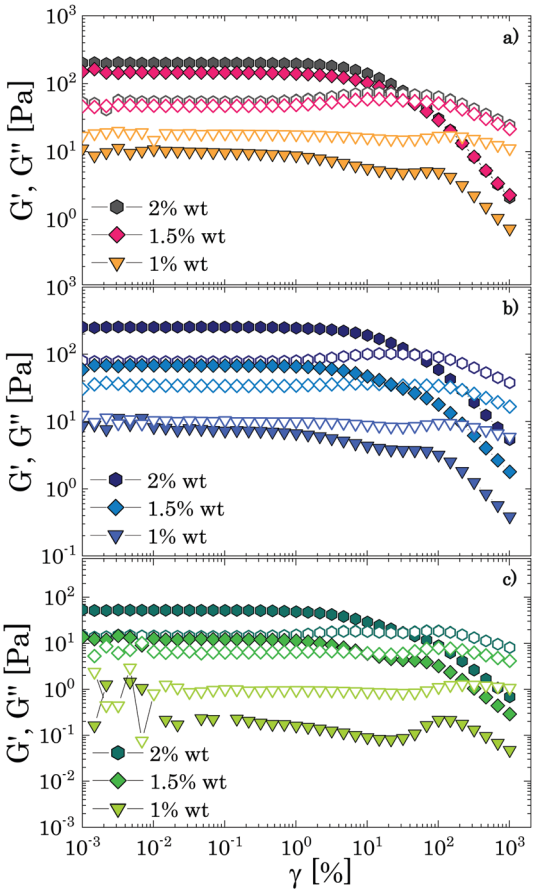

Fig. 7 Strain amplitude dependence of the storage (closed symbols) and loss (hollow symbols) moduli at ω = 1 rad s^{-1} below the fully packed regime for the three different solvents obtained from LAOS experiments: (a) glycerol; (b) PEG/glycerol; (c) PEG.

strains and the shear-thinning behaviour of G' and G'' in the region between the two peaks enlarges and becomes more pronounced.[39] This behaviour is typically associated with destructuring of disordered particle networks or particle cluster networks induced by the attractive interactions, which allow at low strain levels to maintain a yield stress behaviour down to low volume fractions[39,59,69](*e.g.* $\phi \approx 0.2$; however, this value strongly depends on the strength of the attraction[70]).

We replotted the data in Fig. 7 by normalizing G' and G'' with their corresponding plateau values at $\gamma \to 0$ to better reveal the presence of the peaks; the results are shown in Fig. 8. For all different solvents, the same qualitative behaviour is observed. As the mass fraction of Carbopol decreases to the limit of the critical concentration c_c, *i.e.* 2 wt% for P solutions and 1.5 wt% for G and PG solutions, the normalized storage modulus maintains the same shape and monotonically decreases following a smooth sigmoidal trend, whilst the magnitude of the peaks of G'' decreases, and the initial peak observed for densely packed regimes is replaced by a first peak occurring at $\gamma = \gamma_{c1} \approx 10\%$ and by a second peak at $\gamma = \gamma_{c2} \approx 100\%$, which appears more or less pronounced in the three different solvents.

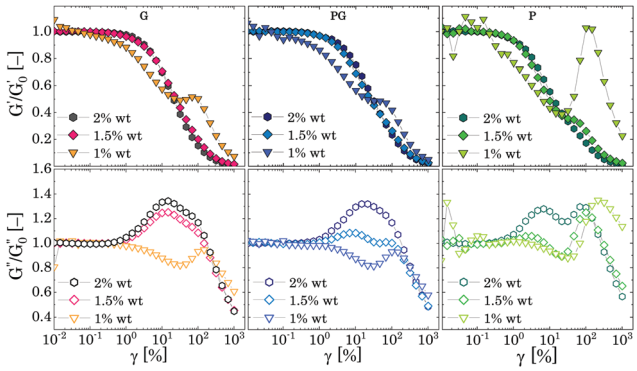

Fig. 8 Normalised G' (upper row graphs) and G'' (lower row graphs) as function of the strain amplitude for the three different solvents.

Nonetheless, as the Carbopol concentration is reduced to 1 wt%, at the frequency tested the elastic contribution becomes lower than the viscous one in the entire range of strains. For G and PG solutions, G'' shows a local depression just after $\gamma \approx \gamma_{c1}$ followed by a temporary recovery at $\gamma \approx \gamma_{c2}$, readily followed by a mild shear thinning decrease. On the other hand, G' decreases almost linearly up to a characteristic strain, slightly lower than γ_{c2}, at which a peak shows, before reaching the viscous terminal behaviour. A similar behaviour is observed for P solutions, although the gap between the magnitude of G'' and G' is more significant and the normalised peaks are more pronounced, as can be observed from Fig. 8.

Steady shear tests applied to the same sample concentrations reveal the presence of a yield stress for all G and PG solutions with Carbopol concentration equal or above 1 wt%, whilst for P solutions the stress plateau has already disappeared for solutions at 1 wt% (Fig. 9). Just above the critical concentration c_c (*i.e.* G and PG solutions at 2 wt%), all samples present a yield stress and the shear stress can be fitted with the HB model, giving a shear-thinning index n_B still close to 0.5. As the samples move away from a densely packed condition, n_B further increases and the flow curves are better fitted with a modified version of the HB model,[4,71] which includes a second power law regime at lower shear rates:

$$\sigma = \sigma_B + k_n\dot{\gamma}^{n_B} + k_p\dot{\gamma}^{n_p} \quad (3)$$

Fitting parameters for all solutions are reported in Table 3. The coefficient n_p increases as the samples move away from the jamming transition, as observed in previous works.[4,71]

As the Carbopol concentration is further decreased, the yield stress disappears and a Newtonian behaviour is observed for $\dot{\gamma} \to 0$, *i.e.*, the stress curves reach an asymptotic slope equal to 1 (Fig. 9), marking the transition from a glassy arrested state to a viscous solution. The transition happens in the range of Carbopol concentrations 1–0.8 wt% for G and PG solutions and 1.5–1 wt% for P solutions, which is consistent with the linear viscoelastic behaviour described in Section 3.1. Note that these ranges of concentrations correspond to apparent volume fractions not lower than 0.62 (which is the value for P solutions at 1 wt%, see Table S2.2 in the ESI†). The flow curves in this

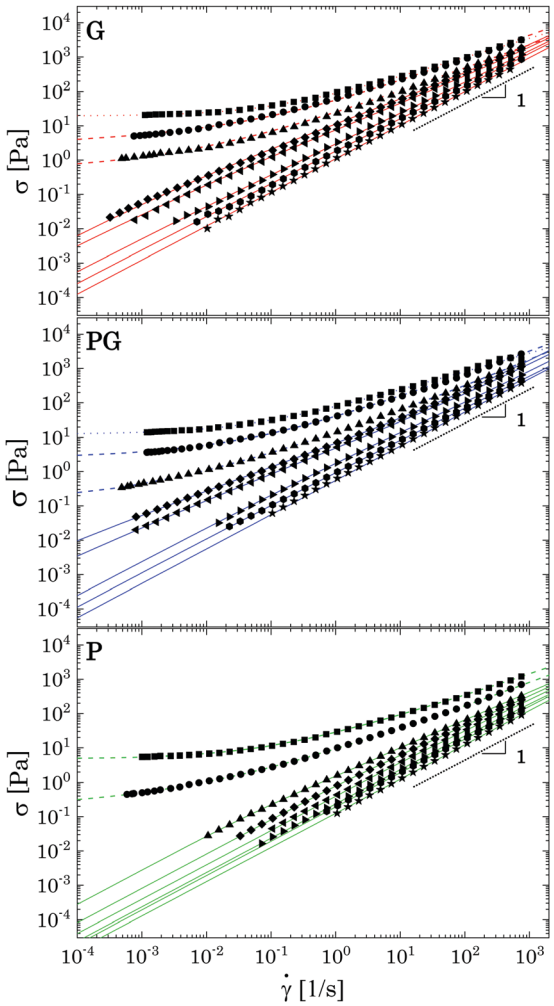

Fig. 9 Flow curves of the samples for decreasing Carbopol mass fraction in three different solvents. For each plot from top to bottom: (2 wt%, 1.5 wt%, 1 wt%, 0.8 wt%, 0.7 wt%, 0.5 wt%, 0.4 wt% and 0.2 wt%). Coloured dotted lines represent fitting of the experimental data with the Herschel–Bulkley model (eqn (2)); dashed lines fitting with the modified HB model (eqn (3)), continuous lines fitting with the Carreau-Yasuda model.

Table 3 Values of the HB parameters obtained from fitting of the experimental flow curves below the densely packed regime

w_c (%)		σ_B (Pa)	k_n (Pa s^{n_B})	n_B (−)	k_p (Pa s^{n_p})	n_p (−)
2	G	19.3	70	0.57	—	—
	PG	12.5	66	0.54	—	—
	P	4.9	3.7	0.76	20	0.52
1.5	G	2.4	37.3	0.68	16.7	0.25
	PG	2.3	29.8	0.67	8.4	0.28
	P	0.19	5.7	0.71	3.5	0.37
1	G	0.43	19.7	0.68	5	0.3
	PG	0.16	5.7	0.81	7.9	0.49
	P	—	—	—	—	—

regime can be fitted with the Carreau-Yasuda model (see S7 ESI† for fitting parameters). All solutions behave as shear-thinning fluids, with shear-thinning indexes that increase with decreasing Carbopol concentration until the Newtonian behaviour is reached in the complete range of shear rates tested.

Overall, the results obtained from LAOS and steady shear measurements indicate that for all solutions a loss of solid-like behaviour is observed as soon as the particle confinement is lost, which is typically observed in soft repulsive systems undergoing a glass transition.[4,51] However, close to the jamming transition, the yielding behaviour is not characterised by a single peak but instead the loss modulus shows two peaks, indicating a more complex particle escaping mechanism. This behaviour suggests the presence of short-range interparticle attractions (*e.g.* van der Waals interactions), which can form disordered particle clusters only when particles are in close contact. At higher particle concentrations, these contacts can extend between clusters, forming larger aggregates that are usually sensitive to the specific shear protocol applied.

To verify this picture, we further investigated the reversibility of the yielding behaviour of samples close to and just below c_c by performing consecutive ascending and descending amplitude sweeps at a fixed frequency of 1 rad s^{-1}. Before each ramp, samples were conditioned by applying a pre-shear at 100 s^{-1} for 60 s, followed by a rest period of 900 s.

In the presence of repulsive particle interactions, the response to nonlinear deformations is expected to be perfectly reversible because there is no significant interconnection between particles and the suspension yields simply by a 'cage' escape mechanism, meaning that, as the deformation is reduced, the initial microstructure is recovered as particles are confined again in the cages, thus showing the same plateau values of G' and G''. By contrast, for attractive particle interactions, the yielding behaviour is extremely sensitive to the shear history that the sample has experienced because of the significant de-structuring that the initial microstructure, characterized by connectivity between single particles, undergoes under flow.[31] In fact, in an ascending amplitude sweep the initial particle network will be progressively broken into smaller clusters until ideally reaching a dispersion of single particles, whilst in a descending ramp, the original strongly interconnected structure will be unable to reform in the time of the experimental ramp, thus causing a reduction of the linear elastic plateau, which can be of one or more orders of magnitude.

For brevity, we report only the results obtained for P solutions at 2 wt% (*i.e.*, close to c_c) and 1.5 wt% (*i.e.*, just below c_c) of Carbopol in Fig. 10, which better highlight the effect of mild particle–particle attractions on the reversibility of the yielding behaviour at the tested frequency. The response to nonlinear deformations is perfectly reversible for both samples only for high strain amplitudes (*i.e.*, $\gamma > \gamma_{c2}$), where the sample is completely yielded and the initial structure has been broken. At lower strains, the linear plateaus of G'' and G' obtained with the descending sweeps for the sample close to the jamming transition (*i.e.*, 2 wt% in Fig. 10) remain in the same order of magnitude, reducing only by a factor of 1.1 and 1.5, respectively. The same results were found for all samples close to the jamming transition, independently of the solvent used (see S8 ESI†).

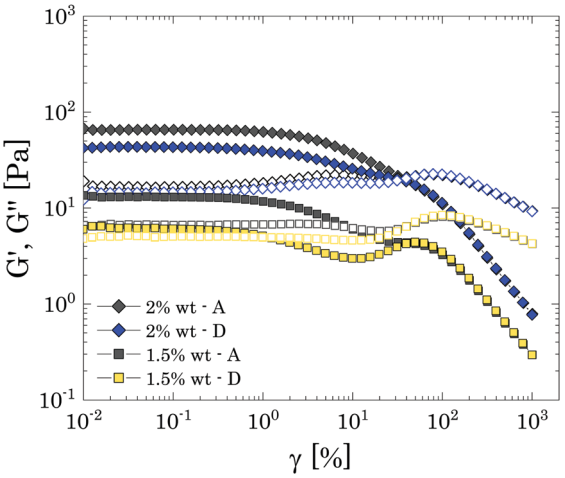

Fig. 10 Ascending (A) and descending (D) amplitude sweeps for P solution close (2 wt%) and below (1.5 wt%) the critical concentration c_c. As usual, closed symbols indicate the storage modulus, whilst hollow symbols the loss modulus.

This modest decrease reveals that, although the initial microstructure is mainly maintained by the topological confinement of the particles, as happens for repulsive systems, there is a small component related to particle–particle interactions, which alters the structure reorganisation in the descending ramp. This is better highlighted at lower particles concentrations, just below the jamming transition (*i.e.* 1.5 wt% in Fig. 10), for which the descending sweep displays a clear loss of the original structure, which is partially recovered at lower strains. These observations resemble what has been already reported by other authors for similar systems.[31] In this previous study, the loss of reversibility was attributed to an increase of the characteristic size of the smallest clusters achievable, which entailed a reduction of the cluster-cluster contacts and therefore of the network strength, resulting in a drop of the elastic plateau of one order of magnitude. In the present case, the results obtained from LAOS experiments indicate a similar mechanism, showing that once the sample has been destructed, it cannot fully recover its initial configuration within the experimental time.

As particle concentration reduces just below the jamming threshold, particle caging begins to fade until solutions no longer present a stress plateau. Nonetheless, since particle concentration is still significant, random clusters can still form in the bulk of the solution between particles that are at close distance, thus explaining the behaviour observed with the LAOS tests for P solutions at 1 wt%, which do not show a yield stress in steady shear tests: as a shear deformation is applied, particle clusters can interact with each other forming bigger aggregates and deform under shear more freely without breaking up. At smaller amplitude strains, the movement of these aggregates will create local pockets of solvent, which cause the local decrease observed in the loss modulus. As the amplitude of the strain applied increases, the aggregates deform up to a certain point at which eventually they break again into smaller clusters.

Just before the breaking point, the aggregates have reached the maximum deformed configuration; in this condition the system is able to accumulate the stress applied as elastic energy, hence showing a peak in the storage modulus, which is then abruptly dissipated after rupture. The interactions between clusters in this regime happen randomly when particles are forced to contact under flow and the absence of a solid-like behaviour at low strains (*i.e.* absence of a yield stress) suggests the lack of a strong interconnected structure spanning the whole bulk of the suspensions.

We conclude that, although the results obtained from LAOS experiments indicate the presence of some interparticle attractions, which influences the yielding mechanism near random packing concentrations, all suspensions undergo a transition from a viscous solution to a glassy state induced by a "cage effect", independently of the solvent used. This confirms that the use of different solvents mainly influences the final swollen state of Carbopol particles and therefore the rheological behaviour of all solutions should be scalable with the particle volume fraction. We point out that, in the range of shear rates investigated, we cannot distinguish clearly a glass transition from the flow curves for the solutions studied; this is likely because, given the limit in the range of shear rates, the flow behaviour of the solutions is sampled in the athermal regime[51]($\tau_T > 1/\dot{\gamma}_{min}$, for all solutions), where any effect related to the thermal energy of the particles is suppressed.

The nature of the interparticle attractions responsible for the rheological behaviour observed is unclear and difficult to predict. Considering their efficacy only at concentrated regimes, they are probably related to van der Waals potentials between swollen particles, which dominate over the repulsive electrostatic and steric interactions only at close particle contact. The qualitative effect on the bulk rheological properties appears to be independent of the solvent, although P solutions show a more noticeable difference in the magnitude of the peaks compared to the other two solvents, as shown in Fig. 8. This could indicate stronger attractive forces in the sole presence of PEG_{400} molecules, which are, however, difficult to explain at this stage. The difference could be related to various aspects, from a worse degree of solvation of the external polymer chains, which would reduce the steric repulsion between particles, to a decrease of the electric double layer due to the worse dielectric properties of PEG_{400} compared to glycerol, which would in turn also partially affect the van der Waals interactions through the Hamaker constant.[42] Further investigations, which are beyond the scope of this work, would be of great interest to understand more deeply the specific interactions responsible for the rheological observations.

3.2.3 Determination of the particle final swollen radius. To estimate the final swollen dimensions of the Carbopol molecules in the three solvents, we first consider the trend of the zero-shear relative viscosity η_r as a function of Carbopol mass concentration. Data for all solvents are reported in Fig. 11. Like what is predicted for hard sphere suspensions at increasing particle volume fraction, the relative viscosity diverges as the critical jamming concentration is approached.

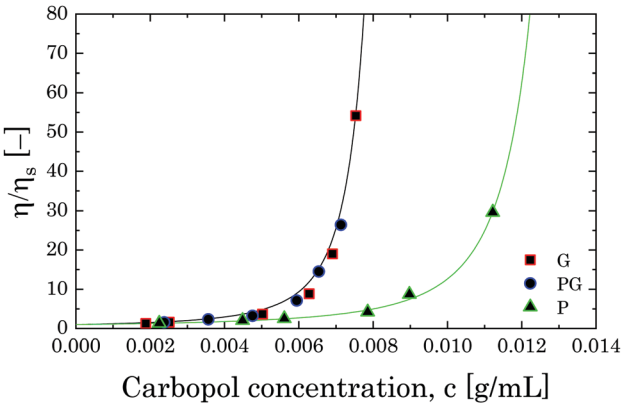

Fig. 11 Relative viscosity as a function of Carbopol concentration for G, PG and P solutions in the semi-dilute regime. The solid lines represent the fitting with eqn (8).

The data for G and PG solutions fall on the same curve, while the values for P solutions diverge at higher Carbopol concentrations. If a linear relation is assumed between the mass concentration c and the final volume fraction ζ of the type:

$$\zeta = k_M c \tag{4}$$

the trends in Fig. 11 suggest a shift in the effective volume fraction of P solutions, which can be directly related to a reduced swelling of Carbopol molecules in PEG. Note that here we denote the apparent volume fraction obtained from the rheological measurements by ζ to distinguish it from the values ϕ acquired from the confocal images. In the assumption that Carbopol particles can be modelled as porous spheres, with initial radius R_{IN}, apparent dry density ρ_p and final swollen radius R_{SW}, eqn (4) can be written as follows:

$$n_p \frac{4}{3}\pi {R_{SW}}^3 = k_M n_p \frac{4}{3}\pi {R_{IN}}^3 \rho_p \tag{5}$$

where n_p is the particle number density per unit volume of suspension. By rearranging eqn (5), the final swollen radius is given by:

$$R_{SW} = R_{IN}(\rho_p k_M)^{1/3} \tag{6}$$

where k_M is the only unknown. Hence, in the limit of validity of eqn (4), k_M can be found by fitting the data reported in Fig. 11 with a theoretical model for the relative viscosity of sphere suspensions. Both sets of data are fitted with the equation derived by Mooney for concentrated suspensions of spherical particles:[72]

$$\eta_r = \exp\left(\frac{2.5\zeta}{1-\lambda\zeta}\right) \tag{7}$$

where, λ is a fitting parameter related to the maximum packing factor that the system can achieve, which for polydisperse systems depends significantly on the particle size distribution. As an indication, $\lambda \approx 1/\zeta_p$, where ζ_p is the volume fraction at maximum packing. The equation derived by Mooney is an extension of the Einstein equation for infinitely diluted systems, which considers the crowding effect of neighbouring particles. It has been developed for hard spheres but it has been successfully applied also to softer systems such as emulsions.[72] By substituting eqn (4) into eqn (7), we obtain the fitting equation:

$$\eta_r = \exp\left(\frac{2.5 k_M c}{1-\lambda k_M c}\right) \tag{8}$$

If we assume that the final value of λ depends only on the polydispersity of the Carbopol particles in the dry state, the same value should be assumed for all solutions and data can be fitted together to obtain the optimal values of λ, $k_M^{(G/PG)}$ and k_M^P (for details about the fitting procedure see S9, ESI†). The data in Fig. 11 can be replotted as a function of the apparent volume fraction ζ (following eqn (4)). The outcome is displayed in Fig. 12, which shows an efficient rescaling of the zero-shear viscosity up to $\zeta \sim 0.5$. Note that the majority of the data are at intermediate volume fractions, where other relations commonly used for dilute dispersions do not apply. For reference, the Batchelor equation[73] (*i.e.* $\eta_r = 1 + 2.5\zeta + 6.2\zeta^2$) is also reported in Fig. 12, clearly showing a significant deviation from Mooney's prediction beyond its limit of validity (*i.e.* around $\zeta \sim 0.2$) (inset in Fig. 12). The final values of the fitting parameters are reported in Table 4, with the corresponding final radii obtained from eqn (6) and the values of the swelling ratio Q_S defined as:

$$Q_S = \frac{V_{SW} - V_{IN}}{V_{IN}} = \left(\frac{R_{SW}}{R_{IN}}\right)^3 - 1 \tag{9}$$

The values of R_{SW} agree with those found from confocal microscopy (reported previously in Section 2.3). In pure glycerol, Carbopol 974NF can swell up to more than 8 times from its initial size, whilst in PEG the swelling is reduced to 5 times. This difference can be attributed to the different degree of ionization that the two solvents induce on Carbopol molecules. For linear chains of uncrosslinked polyacrylic acid, the final conformation of the molecules in a solvent is reported to strongly depend on the

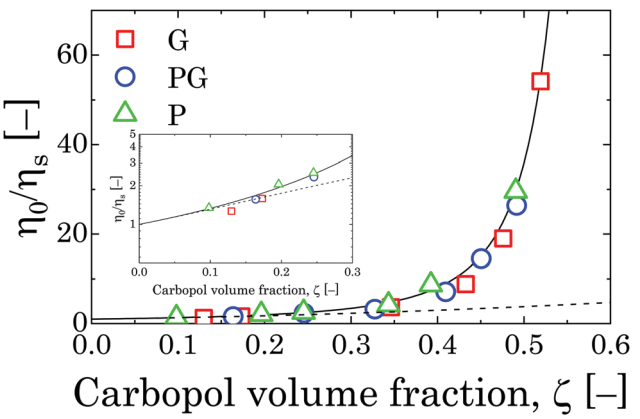

Fig. 12 Relative viscosity rescaled with Carbopol volume fraction ζ for G, PG and P solutions in the semi-dilute regime. The solid line represents the fitting with Mooney's equation,[72] whilst the dashed line is the Batchelor equation.[73] The inset shows the point at which the Batchelor equation starts to deviate from Mooney's.

Table 4 Parameters obtained from fitting of the experimental relative viscosity with eqn (8), final swollen radii, swelling ratio, particle elastic modulus, characteristic time of the thermal fluctuations (recalculated with the updated particle dimensions) and Carbopol concentration c_J and mass fraction w_J corresponding to the apparent volume fraction at the jamming transition (considered as the volume fraction ζ_J at which the relative zero-shear viscosity diverges, *i.e.* $\zeta_J \approx 1/\lambda = 0.769$) for Carbopol particles swollen in the three different solvent

	λ (−)	k_M (mL g^{-1})	R_{SW} (nm)	Q_S (−)	G_p (Pa)	τ_T (s)	c_J (g mL^{-1})	w_J (%)
G		68.9	603	8.4	554	$3.3 \times 10^{+3}$	0.011	0.89
PG	1.3					$1.4 \times 10^{+3}$		0.94
P		43.7	518	5.3	873	$2.4 \times 10^{+2}$	0.0176	1.57

density of the dissociated carboxyl groups distributed along the backbone of the molecule, which alter the conformation due to electrostatic repulsions.[43] In a crosslinked structure, such as that of Carbopol molecules, although the presence of electrostatic repulsions might play a role in inducing an initial unravelling of the collapsed structure, the final swelling degree is controlled by the osmotic pressure between the internal charged environment and the external solvent. In the absence of any neutralizing agent, the effect of each pure solvent is mild but still quite distinguishable, as highlighted by the rheological measurements. Thanks to the higher density in OH groups, glycerol molecules can induce a higher degree of ionization compared to polyethylene glycol thus promoting a more pronounced swelling. Interestingly, when the two solvents are combined, the outcome is equal to what is observed in the sole presence of glycerol.

These findings highlight that the kinetic aspect of the swelling process is critical to the final swollen state achieved. As reported in a previous work,[35] the swelling kinetics of these systems is diffusion-controlled, meaning that smaller molecules with a better affinity with the polymer and a higher capability of transporting charges will preferentially move inside the crosslinked structure of Carbopol. Hence, if the amount of glycerol in solution is enough to swell the majority of the particles, the final swollen average dimension will be equal to that obtained in the pure solvent.

The values found through the rheological measurements are estimated on the assumption that eqn (4) is still valid in the semi-dilute regime (for $0.25 < \zeta < 0.5$) and particles can fully swell to their final equilibrium dimension. Although a reduction of the final particle dimensions surely happens for samples above the jamming transition for steric effects, the predictions of the critical mass fraction w_J at which the jamming transition happens for all solvents (obtained from the volume fraction ζ_J at which the relative zero-shear viscosity diverges, *i.e.* $\zeta_J \approx 1/\lambda = 0.769$) are within the ranges expected from the analysis of the flow curves at higher concentrations, as previously reported in Section 3.2.2. This suggests that our assumption is acceptable in the range of concentration used to fit the Mooney equation. The values of w_J are reported in Table 4 for all solutions.

Determining precisely the particle radius in microgel systems such as Carbopol above the semi-dilute regime can be quite challenging because of their ability to de-swell and deform to accommodate a higher number of particles, thus altering their original dimension and the actual particle volume fraction, which should be used to scale all the rheological properties.

Despite the lack of accuracy of eqn (4) above the semi-dilute regime, it is possible to use the fitting parameter k_M to estimate the particle elastic modulus G_p (which can be calculated from the parameter K_p found in Section 3.1, *i.e.* $G_p = K_p/k_M$) and the apparent volume fraction ζ (*i.e.*, $\zeta = k_M c$) and verify that the flow behaviour for all solutions follows the same scaling laws predicted for athermal suspensions of soft elastic particles with no significant attractive forces in all the regimes investigated.

Close to the jamming point, all flow curves can be collapsed on two separate branches, one above and the other below the jamming transition, by scaling the shear stress σ and the shear rate $\dot{\gamma}$ as $\sigma/(E|\zeta - \zeta_J|^{\Delta})$ and $\eta_s\dot{\gamma}/(E|\zeta - \zeta_J|^{\Gamma})$, respectively.[2,51,65,74] In the scaling relations, E represents the elasticity of the particulate material (*i.e.*, G_p) and Δ and Γ are power law parameters that for Hertzian particles theoretically have the values of 2 and 4,[65] respectively.

Hence, all data presented in Fig. 9 with concentrations close to the jamming transitions (*i.e.* for % mass fractions 0.7% $< w <$ 2 wt% for G and PG solutions and 1 wt% $< w <$ 2 wt%) can be replotted by applying the scaling laws above (see Table 4 for a summary of the parameters used for scaling). The outcome is shown in Fig. 13. Independently of the solvent used, it is possible to collapse all flow curves close to the jamming point in two separate branches, one above and the other below jamming, thus confirming that the nature of the liquid-to-solid transition is mainly dominated by a jamming dynamics and that different solvents mainly influence the final swollen dimensions of the polymer particles.

The scaling above derives from the specific nature of the jamming transition and does not hold far above or below the jamming point. Hence the flow curves obtained in a densely

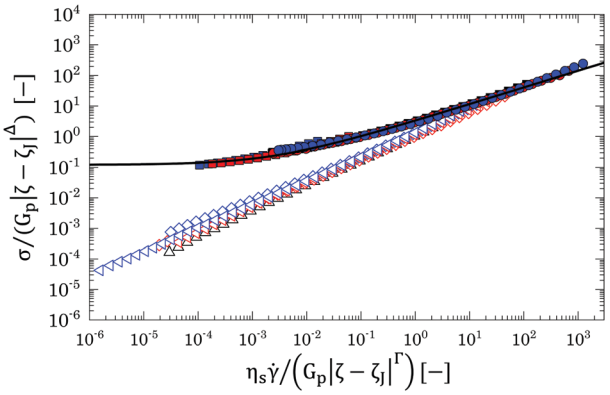

Fig. 13 Scaled version of Fig. 9 for G (red), PG (blue) and P (black) solutions, down to concentrations of 0.7 wt% for G and PG solutions and of 1 wt% for P solutions. All concentrations above the jamming transition (*i.e.* with % mass fractions $w > w_J$) are reported in closed symbols, whilst below the jamming point are reported in hollow symbols. The dashed line is the theoretical HB fitting with power law exponent equal to 0.53.

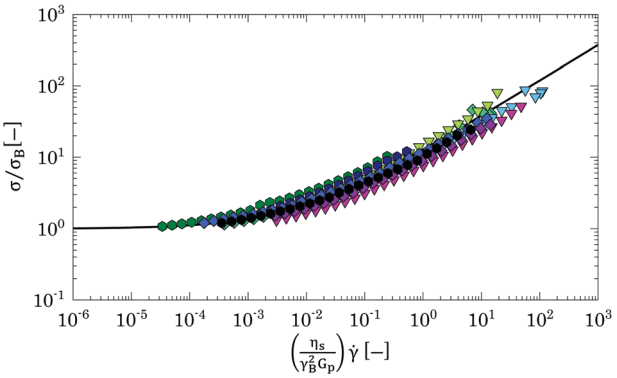

Fig. 14 Collapsed flow curves in the densely packed regime. Symbols legend is the same as in Fig. 6. The black line represents the fitting with eqn (10).

packed regime, which are far above this point, should be collapsed considering a different scaling. At these high volume fractions, the flow behaviour is controlled by the competition between the elastic restoring force and the viscous forces between particle facets.[67,75] This physical picture is well captured by a micromechanical model developed by Seth and co-workers,[67] for athermal suspensions of soft elastic particles, which incorporates the effects of elastic interactions with the hydrodynamic contributions resulting from particles sliding. The model predicts a constitutive equation for the flow curve of a packed dispersion of elastic particles, with particle contact modulus E^*, dispersed in a solvent of viscosity η_s, of the HB type:

$$\frac{\sigma}{\sigma_B} = 1 + k\left(\dot{\gamma}\frac{\eta_s}{E^*{\gamma_B}^2}\right)^{1/2}; k \equiv (k_n/\sigma_B)\left(\frac{E^*{\gamma_B}^2}{\eta_s}\right)^{1/2} \quad (10)$$

where, σ_B and γ_B are the yield stress and strain, respectively, which are linked by the relation for linear elastic solids and k is the dimensionless consistency index. Therefore, we can replot the flow curves of Fig. 6 using the dimensionless shear stress σ/σ_B and the dimensionless shear rate $\dot{\gamma}\eta_s/E^*{\gamma_B}^2$, where γ_B is calculated from the HB yield stress (*i.e.* $\gamma_B = \sigma_B/G_0'$) and $E^* = G_p$. The result of the scaling is shown in Fig. 14. The curves overlap independently of the solvent used and collapse (within an error $<20\%$) on the theoretical prediction (black line), thus showing that all samples behave as suspensions of jammed soft spherical particles and, independently of the real dimension and degree of deformation of the Carbopol particles, their flow behaviour can be scaled with the particle elastic modulus G_p obtained from the estimated parameter k_M.

4 Conclusions

The effect of non-aqueous solvents on the swelling behaviour and mutual interactions of Carbopol particles has been investigated to understand better how these phenomena impact the rheological design of non-aqueous formulations.

The rheological properties of dispersions of a highly crosslinked Carbopol polymer (Carbopol 974P NF) in glycerol (G), PEG_{400} (P) and a mixture of the two (PG) are mapped from the dilute to the densely packed regime. At increasing Carbopol concentration, all solutions display the typical viscoelastic properties of mildly attractive soft particle suspensions. A clear shift in the onset of the jamming transition occurs when pure PEG_{400} is used as solvent, whilst the liquid-to-solid transition is the same for G and PG dispersions. Nevertheless, once the jammed state is reached, the elastic modulus is simply scalable with the polymer mass fraction, regardless of the solvent used. These results suggest that the use of different solvents clearly influences the swelling behaviour of Carbopol molecules, which is reflected in a higher characteristic jamming concentration for P solutions, yet without altering the interparticle interactions in the limit of small deformations.

The typical behaviour of a fully packed suspension of soft particles is also confirmed by the response to non-linear deformations from both LAOS and steady shear experiments. Above the close packing regime, when particles are significantly deformed against their neighbours, all dispersions behave as a packed dispersion of elastic deformable particles and the flow behaviour is mainly regulated by the interplay between the elastic interaction between particles in direct contact and hydrodynamic interactions originating from particles sliding. Below the close packing concentration, LAOS experiments reveal the presence of short-range attractive forces between Carbopol particles, which are highlighted by the two-step yielding mechanism of the loss modulus at increasing shear deformations. Nonetheless, the loss of a yield stress just below the jamming transition suggests that the attractions are only significant when particles are in close contact and the liquid-to-solid transition for all solvents considered is mainly "cage" driven. Carbopol particles swell up to more than 8 times their initial size in G and PG dispersions, whilst in PEG the swelling is reduced to 5 times. These findings, confirmed also by confocal microscopy, highlight that, even in the absence of water, the main driving mechanism that controls the final swollen conformation is the degree of ionization induced by the solvent on Carbopol molecules. Furthermore, in the presence of co-solvents the kinetic aspect of the swelling process is critical to the final swollen state achieved, as highlighted by the equal swelling degree obtained for G and PG dispersions. The swelling kinetics of these systems are diffusion-controlled, thus if one of the solvents presents better permeability in the carbomer network and is present in amount sufficient to swell the majority of the particles, the final swollen average dimension of the particle is equal to what is obtained in the presence of that solvent alone.

Once the average particle dimension is known, the flow properties above and below jamming can be scaled for all solvents simply with an apparent particle volume fraction, showing a flow behaviour consistent with soft particle systems in the athermal regime, with some anomalies observed at significantly high particle concentrations. These results highlight that, even if typically the morphology of Carbopol molecules is described as quite irregular, thanks to its high crosslinking degree, Carbopol 974P NF, as opposed to other

types with a lower crosslinking degree, can be well approximated to a soft spherical particle until densely packed regimes are reached. In these regimes, the rheological behaviour becomes more sensitive to particles irregularities (*e.g.* presence of dangling ends, possible uneven distribution of the crosslinking density or of functional groups), which influences the interactions between the particles when they are forced to close contact. These effects are complex to clearly address, given the commercial nature of the material, and further investigations would be of great interest to elucidate the anomalies observed at high particle concentrations.

Conflicts of interest

There are no conflicts to declare.

Acknowledgements

The authors would like to acknowledge Ollie Hughes and Prof. Paul Bartlett from the School of Chemistry of the University of Bristol (UK) for providing the labelled Carbopol for the confocal imaging and GlaxoSmithKline Consumer Healthcare and the EPSRC Future formulations grant CORAL (EP/N024915/1) for the financial support given to this project.

References

1 D. Vlassopoulos and M. Cloitre, *Curr. Opin. Colloid Interface Sci.*, 2014, **19**, 561–574.
2 D. Bonn, M. M. Denn, L. Berthier, T. Divoux and S. Manneville, *Rev. Mod. Phys.*, 2017, **89**, 1–40.
3 L. A. Lyon and A. Fernandez-Nieves, *Annu. Rev. Phys. Chem.*, 2012, **63**, 25–43.
4 C. Pellet and M. Cloitre, *Soft Matter*, 2016, **12**, 3710–3720.
5 P. H. T. Uhlherr, J. Guo, C. Tiu, X. M. Zhang, J. Z. Q. Zhou and T. N. Fang, *J. Nonnewton. Fluid Mech.*, 2005, **125**, 101–119.
6 C. J. Dibble, M. Kogan and M. J. Solomon, *Phys. Rev. E: Stat., Nonlinear, Soft Matter Phys.*, 2006, **74**, 1–11.
7 T. Eckert and E. Bartsch, *Phys. Rev. Lett.*, 2002, **89**, 20–23.
8 V. Prasad, V. Trappe, A. D. Dinsmore, P. N. Segre, L. Cipelletti and D. A. Weitz, *Faraday Discuss.*, 2003, **123**, 1–12.
9 R. Borrega, M. Cloitre, I. Betremieux, B. Ernst and L. Leibler, *Europhys. Lett.*, 1999, **47**, 729–735.
10 P. Menut, S. Seiffert, J. Sprakel and D. A. Weitz, *Soft Matter*, 2012, **8**, 156–164.
11 H. Bachman, A. C. Brown, K. C. Clarke, K. S. Dhada, A. Douglas, C. E. Hansen, E. Herman, J. S. Hyatt, P. Kodlekere, Z. Meng, S. Saxena, M. W. Spears, N. Welsch and L. A. Lyon, *Soft Matter*, 2015, **11**, 2018–2028.
12 A. Le Grand and G. Petekidis, *Rheol. Acta*, 2008, **47**, 579–590.
13 P. Lefrançois, E. Ibarboure, B. Payré, E. Gontier, J.-F. Le Meins and C. Schatz, *J. Appl. Polym. Sci.*, 2015, **132**, 1–7.
14 L. Boulmedarat, J. L. Grossiord, E. Fattal and A. Bochot, *Int. J. Pharm.*, 2003, **254**, 59–64.
15 G. Bonacucina, S. Martelli and G. F. Palmieri, *Int. J. Pharm.*, 2004, **282**, 115–130.
16 S. J. Curran, R. E. Hayes, A. Afacan, M. C. Williams and P. A. Tanguy, *J. Food Sci.*, 2002, **67**, 176–180.
17 J. M. Piau, *J. Nonnewton. Fluid Mech.*, 2007, **144**, 1–29.
18 T. Divoux, D. Tamarii, C. Barentin and S. Manneville, *Phys. Rev. Lett.*, 2010, **104**, 1–4.
19 F. K. Oppong and J. R. de Bruyn, *Rheol. Acta*, 2011, **50**, 317–326.
20 J. O. Carnali and M. S. Naser, *Colloid Polym. Sci.*, 1992, **270**, 183–193.
21 D. Lee, I. A. Gutowski, A. E. Bailey, L. Rubatat, J. R. de Bruyn and B. J. Frisken, *Phys. Rev. E: Stat., Nonlinear, Soft Matter Phys.*, 2011, **83**, 031401.
22 I. A. Gutowski, D. Lee, J. R. de Bruyn and B. J. Frisken, *Rheol. Acta*, 2012, **51**, 441–450.
23 B. D. Jofore, P. Erni, G. Vleminckx, P. Moldenaers and C. Clasen, *Rheol. Acta*, 2015, **54**, 581–600.
24 T. Bhattacharjee, C. P. Kabb, C. S. O'Bryan, J. M. Urueña, B. S. Sumerlin, W. G. Sawyer and T. E. Angelini, *Soft Matter*, 2018, **14**, 1559–1570.
25 B. Barry and M. Meyer, *Int. J. Pharm.*, 1979, **2**, 1–25.
26 R. J. Ketz, R. K. Prud'homme and W. W. Graessley, *Rheol. Acta*, 1988, **27**, 531–539.
27 T. Divoux, V. Grenard and S. Manneville, *Phys. Rev. Lett.*, 2013, **110**, 018304.
28 M. Dinkgreve, M. Fazilati, M. M. Denn and D. Bonn, *J. Rheol.*, 2018, **62**, 773–780.
29 G. J. Donley, J. R. de Bruyn, G. H. McKinley and S. A. Rogers, *J. Nonnewton. Fluid Mech.*, 2019, **264**, 117–134.
30 J. Y. Kim, J. Y. Song, E. J. Lee and S. K. Park, *Colloid Polym. Sci.*, 2003, **281**, 614–623.
31 Z. Shao, A. S. Negi and C. O. Osuji, *Soft Matter*, 2013, **9**, 5492–5500.
32 R. Barreiro-Iglesias, C. Alvarez-Lorenzo and A. Concheiro, *Int. J. Pharm.*, 2003, **258**, 165–177.
33 L. L. Hench, *J. Mater. Sci.: Mater. Med.*, 2006, **17**, 967–978.
34 P. R. Varges, C. M. Costa, B. S. Fonseca, M. F. Naccache and P. R. De Souza Mendes, *Fluids*, 2019, **4**, 1–20.
35 S. Migliozzi, P. Angeli and L. Mazzei, *Colloids Surf., A*, 2019, **577**, 84–95.
36 J. S. Chu, D. M. Yu, G. L. Amidon, N. D. Weiner and A. H. Goldberg, *Pharm. Res.*, 1992, **9**, 1659–1663.
37 K. Miyazaki, H. M. Wyss, D. A. Weitz and D. R. Reichman, *Europhys. Lett.*, 2006, **75**, 915–921.
38 V. Carrier and G. Petekidis, *J. Rheol.*, 2009, **53**, 245–273.
39 N. Koumakis and G. Petekidis, *Soft Matter*, 2011, **7**, 2456–2470.
40 E. M. Furst and J. P. Pantina, *Phys. Rev. E: Stat., Nonlinear, Soft Matter Phys.*, 2007, **75**, 050402.
41 K. N. Pham, G. Petekidis, D. Vlassopoulos, S. U. Egelhaaf, W. C. K. Poon and P. N. Pusey, *J. Rheol.*, 2008, **52**, 649–676.
42 C. N. Likos, *Phys. Rep.*, 2001, **348**, 267–439.
43 A. Laguecir, S. Ulrich, J. Labille, N. Fatin-Rouge, S. Stoll and J. Buffle, *Eur. Polym. J.*, 2006, **42**, 1135–1144.
44 O. H. Hughes and P. Bartlett, personal communication.

45 B. Géraud, L. Jørgensen, C. Ybert, H. Delanoë-Ayari and C. Barentin, *Eur. Phys. J. E: Soft Matter Biol. Phys.*, 2017, **40**, 1–10.
46 I. W. Hamley, *Introduction to Soft Matter*, John Wiley & Sons, Ltd, Chichester, 2007.
47 P. Sollich, *Phys. Rev. E: Stat. Phys., Plasmas, Fluids, Relat. Interdiscip. Top.*, 1998, **58**, 738–759.
48 A. J. Liu, S. Ramaswamy, T. G. Mason, H. Gang and D. A. Weitz, *Phys. Rev. Lett.*, 1996, **76**, 3017–3020.
49 J. J. Liétor-Santos, B. Sierra-Martín and A. Fernández-Nieves, *Phys. Rev. E: Stat., Nonlinear, Soft Matter Phys.*, 2011, **84**, 1–4.
50 G. M. Conley, C. Zhang, P. Aebischer, J. L. Harden and F. Scheffold, *Nat. Commun.*, 2019, **10**, 1–8.
51 A. Ikeda, L. Berthier and P. Sollich, *Soft Matter*, 2013, **9**, 7669–7683.
52 F. Di Lorenzo and S. Seiffert, *Macromolecules*, 2013, **46**, 1962–1972.
53 D. A. Sessoms, I. Bischofberger, L. Cipelletti and V. Trappe, *Philos. Trans. R. Soc., A*, 2009, **367**, 5013–5032.
54 T. G. Mason and D. A. Weitz, *Phys. Rev. Lett.*, 1995, **75**, 2770–2773.
55 S. E. Paulin, B. J. Ackerson and M. S. Wolfe, *J. Colloid Interface Sci.*, 1996, **178**, 251–262.
56 T. G. Mason, M. D. Lacasse, G. S. Grest, D. Levine, J. Bibette and D. A. Weitz, *Phys. Rev. E: Stat. Phys., Plasmas, Fluids, Relat. Interdiscip. Top.*, 1997, **56**, 3150–3166.
57 F. Scheffold, P. Díaz-Leyva, M. Reufer, N. Ben Braham, I. Lynch and J. L. Harden, *Phys. Rev. Lett.*, 2010, **104**, 1–4.
58 H. Senff and W. Richtering, *J. Chem. Phys.*, 1999, **111**, 1705–1711.
59 M. Laurati, G. Petekidis, N. Koumakis, F. Cardinaux, A. B. Schofield, J. M. Brader, M. Fuchs and S. U. Egelhaaf, *J. Chem. Phys.*, 2009, **130**, 134907.
60 A. Ghosh, G. Chaudhary, J. G. Kang, P. V. Braun, R. H. Ewoldt and K. S. Schweizer, *Soft Matter*, 2019, **15**, 1038–1052.
61 J. R. Seth, M. Cloitre and R. T. Bonnecaze, *J. Rheol.*, 2006, **50**, 353–376.
62 M. Cloitre, R. Borrega, F. Monti and L. Leibler, *Phys. Rev. Lett.*, 2003, **90**, 068303.
63 M. Dinkgreve, J. Paredes, M. M. Denn and D. Bonn, *J. Nonnewton. Fluid Mech.*, 2016, **238**, 233–241.
64 F. Rouyer, S. Cohen-Addad and R. Höhler, *Colloids Surf., A*, 2005, **263**, 111–116.
65 K. N. Nordstrom, E. Verneuil, P. E. Arratia, A. Basu, Z. Zhang, A. G. Yodh, J. P. Gollub and D. J. Durian, *Phys. Rev. Lett.*, 2010, **105**, 1–4.
66 B. M. Erwin, M. Cloitre, M. Gauthier and D. Vlassopoulos, *Soft Matter*, 2010, **6**, 2825–2833.
67 J. R. Seth, L. Mohan, C. Locatelli-Champagne, M. Cloitre and R. T. Bonnecaze, *Nat. Mater.*, 2011, **10**, 838–843.
68 M. Laurati, S. U. Egelhaaf and G. Petekidis, *J. Rheol.*, 2011, **55**, 673–706.
69 R. Buscall, P. D. Mills, R. F. Stewart, D. Sutton, L. R. White and G. E. Yates, *J. Nonnewton. Fluid Mech.*, 1987, **24**, 183–202.
70 S. A. Shah, Y. L. Chen, K. S. Schweizer and C. F. Zukoski, *J. Chem. Phys.*, 2003, **119**, 8747–8761.
71 M. Siebenbürger, M. Fuchs, H. Winter and M. Ballauff, *J. Rheol.*, 2009, **53**, 707–726.
72 M. Mooney, *J. Colloid Sci.*, 1951, **6**, 162–170.
73 G. K. Batchelor, *J. Fluid Mech.*, 1977, **83**, 97–117.
74 P. Olsson and S. Teitel, *Phys. Rev. Lett.*, 2012, **109**, 1–5.
75 T. Liu, F. Khabaz, R. T. Bonnecaze and M. Cloitre, *Soft Matter*, 2018, **14**, 7064–7074.